Low Frequency Observations of the Quiet Sun: a Review

Pierre Lantos
CNRS and Observatoire de Paris, Section d'Astrophysique de Meudon, 92195-Meudon Cedex, France
E-mail: pierre.lantos@obspm.fr

Abstract

We present a review of the results obtained on the quiet sun at long decimeter, meter and decameter wavelengths with radioheliographs. Similarities and differences of the radio corona with the corona seen at other wavelengths are analysed. Large-scale structures including coronal holes, the coronal plateau (the radio counterpart of the coronal plasma sheet) and the background quiet sun are considered. The sources of the slowly varying component are identified and described. The importance of low frequency observations of the sun, in addition to X-ray and EUV observations, is pointed out for a better understanding of coronal and solar-terrestrial physics.

Key words: Quiet sun, solar corona, radio observations, coronal holes, coronal streamers.

1. Introduction

During the recent years there has been a considerable renewal of interest in the quiet sun. This is due to the launch of satellites extending again the range of observations to X-ray and EUV wavelengths, two decades after the Skylab mission. Among the reasons for this international space observation program, is the importance of solar observations in improving our knowledge of solar-terrestrial physics. As the corona is the interface between the sun and the interplanetary medium, this new context has reinforced the interest of studying not only eruptive phenomena, but also the quiet corona. Indeed, it should be recalled that 90 % of the time the geomagnetic activity is dominated by the effects of coronal structures rather than flares and CME's (Simon and Legrand 1992).

The low frequency range considered here extends from 400 MHz ($\lambda = 0.7$ meter) to 30 MHz ($\lambda = 10$ meters). According to reference mean models of the corona (Saito 1970 1972), this range corresponds to sun center distances from the chromosphere-corona transition region (CCTR) to about 1.2 $R_\odot$ in the coronal holes, to 1.6 $R_\odot$ in quiet regions and to 2 solar radii in streamers. Starting in the 1950's with aperture synthesis interferometers (Cambridge, Carnegie Institution) and eclipse measurements, the observation of the shape and brightness temperature of the quiet sun at long-decimeter, meter and decameter wavelengths has been extended to regular observations of the so-called slowly varying component (SVC) thanks to interferometers. This review will be mostly restricted to observations obtained with radioheliographs which give, on a regular basis, two-dimensional maps of the Sun. It is nevertheless fair not to underestimate the work done before 1980 with a number of other instruments. Earlier works have been reviewed by Kundu (1965), Lantos (1980) and Sheridan and McLean (1985). Pioneering studies have been done with the Culgoora Radioheliograph in the 1970's. Nevertheless only a limited number of quiet sun observations have been published. After 1980, the Sun has been regularly observed at decameter wavelengths by the Clark Lake (up to 1987) and Gauribidanur (e.g. Sastry 1994) instruments. At long-decimeter and meter wavelengths, maps have been obtained with the Nançay Radioheliograph and with the VLA, using aperture synthesis methods. Since 1996 the Nançay Radioheliograph provides two-dimensional maps with a time resolution of a few minutes (Kerdraon and Delouis 1997) but the spatial resolution is lower than with the synthesis method which is still in use.

Analysis of data shows different quiet sun brightness distributions between long decimeter (frequencies from 450 to 300 MHz) and meter wavelengths. At the same time between 160 MHz and 80 MHz, the origin of the SVC is changing. For these reasons we will consider separately the three ranges, using the term "decameter wavelengths" (somewhat arbitrarily) for the frequencies below 100 MHz.

2. Overview of Low Frequency Observations of the Quiet Sun

The comparison of the information on the corona provided by observations in X-ray, EUV, optical and radio low frequency ranges, clearly shows the specific advantages and limitations of the radio observations. There are many

well known limitations to radio observations: (1) absence of spectral lines, (2) coronal refraction which complicates the measurements of the location of the SVC sources at longer wavelengths and (3) much lower spatial resolution than with X-ray and EUV imagers. The spatial resolution of 3-kilometer class instruments (Culgoora, Clark Lake or Nançay) is about 1 arc minute at 160 MHz. Thus the East-West resolution is in the order of 0.4 arc minute at 410 MHz and 5.5 arc minutes at 30 MHz. Nevertheless it is generally agreed that because of the large sizes of the quiet sun emission sources at long wavelengths, this class of instruments has a resolution not much worse than the source size. Indeed, with higher resolution at 327 MHz, Lang et al. (1988), measured sources sizes of 50 ″ by 200 ″. The VLA, with a baseline of about 30 kilometers, may provide up to 5 arc seconds resolution at 327 MHz, but in this case the field of view is very limited. Most of the observations have been done with VLA configurations giving spatial resolution in the order of arc minute at 327 MHz. Depending on the wavelength, on the location of the instrument and on the season, the changing ionospheric refraction (due to ionospheric gravity waves) may complicate the precise pointing of the radio instruments (e.g. Mercier 1996). Finally, when the earth rotation aperture synthesis techniques are used, strong noise storms can prevent the computation of radio maps, because the noise storm intensity varies strongly during the day.

The high sensitivity of the radio waves to the medium and small-scale density inhomogeneities of the corona is both a limitation and an advantage, compared to the X-ray, EUV and optical ranges. On the one hand this highly complicates the radio diagnostic and thus the comparison of the data with the models is still in its infancy. On the other hand, the radio rays collect in this way more information on the corona than optically thin radiations. This is shown by the corona radio-sounding techniques with galactic sources and spacecraft signal generators (e.g. Bird and Edenhofer 1990).

In the quiet sun and SVC the emission mechanism involved is free-free emission (except for faint noise storms). Thus the observed radio brightness temperature is independent of abundances and ionization equilibrium, and the radiative transfer is easily computed for a given model. Nevertheless, one of the most serious advantages of the radio observations of the quiet sun is related to the altitudes observed on the disk, which are different at different wavelengths, giving a 3-dimensional view of the corona. Even more important is the fact that the radio instruments at low frequencies can observe on the solar disk at much higher altitudes than X-ray and EUV imagers do.

Figure 1 illustrates similarities and differences between X-ray images and radio maps at long decimeter and meter

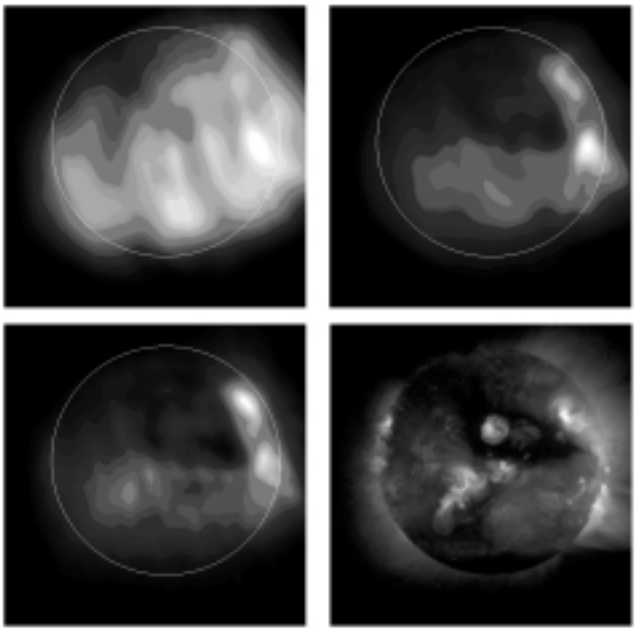

Fig. 1.. Observations of the quiet sun on 26 May 1992 with the Nançay Radioheliograph at 164 MHz (upper left), 327 MHz (upper right) and 410 MHz (lower left). The Yohkoh image is shown at the lower right panel. Courtesy C. E. Alissandrakis and the Yohkoh Team.

wavelengths. The radio maps were obtained with the Nançay Radioheliograph at 164 MHz (upper left), at 327 MHz (upper right) and at 410 MHz (lower left); the figure also shows the corresponding X-ray image from Yohkoh SXT. Let us recall that Yohkoh observes mostly regions with temperature greater than 2 million degrees, while the radio sees also lower temperature regions. The maps at long-decimeter wavelengths show large-scale structures similar to those of the X-ray image. At 410 MHz, coronal holes (north and south) have the same shape as in X-rays. Note also that the faint active region within the northern coronal hole is also visible at 410 MHz. Medium size enhanced emissions (slowly varying component sources in the southeastern quadrant) have the same location as the brightest loops in X-rays. Nevertheless the two bright radio sources seen on the northwestern limb are faint noise storm continuum emissions (non-thermal in nature). Finally, it is important to note that the map at 164 MHz differs from the one at 410 MHz in particular with respect to locations of the thermal enhancements. Decameter maps differ also gradually from maps at meter wavelengths (Lantos et al. 1987). This short discussion illustrates two statements given at the end of the preceding paragraph. On one hand the radio brightness distribution, in the range from 410 MHz to 30 MHz, shows important changes with altitude in the structure of the corona. On the other hand, because of the similarity of X-ray images with 410 MHz maps, longer wavelengths are likely emitted on the disk in loops at higher altitudes (and at lower densities) than the regions observed with X-rays.

3. Large Scale Structures of the Solar Corona

3.1. Coronal Holes

Coronal holes are important structures of the quiet sun for two reasons. On one hand they trace the large-scale structure of the open magnetic field and, on the other, they are the source of the high-speed solar wind streams. In turn, the high-speed solar wind disturbs the magnetosphere and triggers recurrent geomagnetic storms (Zirker 1977).

Because of their lower density, coronal holes are observed as brightness depressions from centimeter to meter wavelengths. Two-dimensional observations of coronal holes at long decimeter and meter wavelengths have been published by Dulk and Sheridan (1974), Dulk et al. (1977), Palagi and Patriarchi (1979), Alissandrakis et al. (1985), Lantos et al. (1987, 1992), Alissandrakis and Lantos (1996). Because of refraction effects (and lower resolution) their boundaries are not as precise at long wavelengths as in EUV or X-rays. In addition, as the radio emission is sensitive to low temperature coronal loops, some intrinsic differences in the boundaries of the holes also exist.

At decameter wavelengths, coronal holes may be seen entirely in emission (Dulk and Sheridan 1974) or as brightness temperature depressions (Dulk et al. 1977). Figure 2 shows meter and decameter maps obtained with the Nançay and Clark Lake instruments (Lantos et al. 1987). The map on the left is at 169 MHz, with a brightness temperature at the center of the disk of about 6.5 10^5 K. The other map, at 50 MHz, has a central brightness temperature of

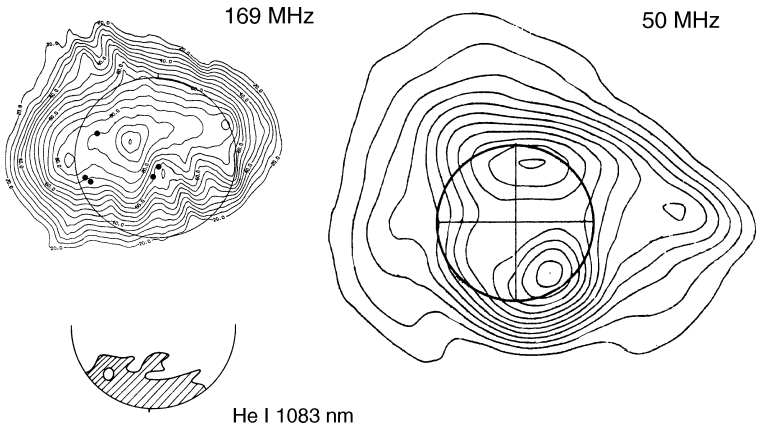

Fig. 2.. Quiet sun brightness distribution on 5 July 1982 at 169 MHz (Nançay Radioheliograph) and 50 MHz (Clark Lake Radioheliograph). The outline of a coronal hole observed at 1083 nm (Kitt Peak Observatory) is given for comparison.

3.5 10^5 K. An extended coronal hole is present in the south hemisphere (see the He I 1083 nm hole drawing on the figure). It manifests itself at meter wavelength by brightness temperatures less than 4 10^5 K on the disk, to be compared with the 7 10^5 K symmetrically at the other hemisphere. At decameter wavelength, the southern bright source is likely associated with the coronal hole. The brightness temperature of the source is about 2 10^5 K above the disk center temperature given previously. Other maps obtained on the same day show that the emission becomes more and more prominent as the wavelength rises. Kundu et al. (1987) have published examples of coronal holes seen as brightness depressions at three decameter wavelengths. Figure 3 (left side) shows an observation at 73.8 MHz. On this particular day, the brightness depression is well located above the coronal hole delineated with large dots. But this is not generally the case, as mentioned by Kundu et al.. Instead of the explanation in terms of large-scale structural details of the low corona given by the authors, we would prefer to invoke refraction of radio rays. Indeed, near a coronal hole, an unexpected emission source is well visible beyond the limb in radial direction. The authors mention that no streamer is detected at the corresponding location on coronagraph pictures. Thus we suspect that this source is also associated to the coronal hole. Indeed the same close association could be noticed at the three frequencies on all the maps available during the passage of the hole on the disk.

Introducing scattering on small-scale density structures, Riddle (1974) and Hoang and Steinberg (1977) pointed out that, under certain conditions, electron density depletions might lead to enhanced radio emission at decameter wavelengths. This would explain coronal holes seen in emission. Nevertheless, without introducing scattering, Alissandrakis (1993) has simulated simultaneous presence of brightness depression and emission above a coronal hole (Figure 3, right side). His model involves a cool density depression embedded in a homogeneous corona. The bright region between the hole and the limb is due to rays propagating almost perpendicularly to the density gradient, penetrating deeper into the low corona and accumulating sufficient optical depth.

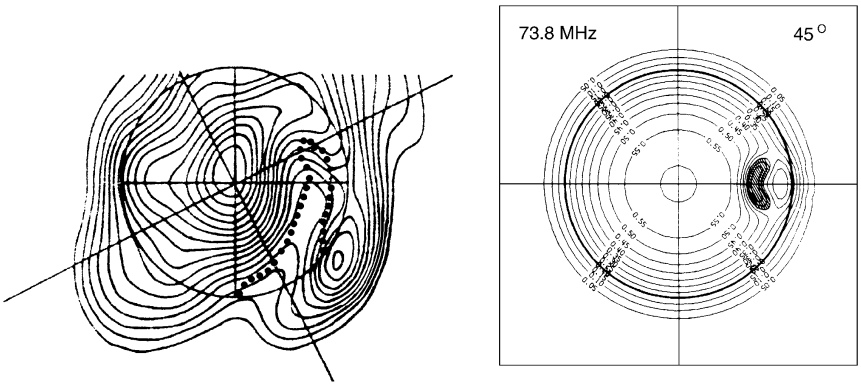

Fig. 3.. Observation of a coronal hole on 21 October 1984 at 73.8 MHz (Clark Lake Radioheliograph, left). On the right side, a model simulating the simultaneous emission and brightness depression in a coronal hole.

Precise measurements of the brightness temperature are essential for the interpretation in terms of models, but they are rather difficult because radioheliographs are complex instruments. Figure 4 summarises observations of coronal hole brightness temperatures (small squares). The open squares are estimates obtained without two-dimensional observations. The corresponding brightness temperatures and references are given in Table 1. Some of the older values have been recalibrated (see Lantos 1980) in the Baars and Hartsuijker (1972) scale or corrected for N-S center to limb effect. In addition to the observed values of hole brightness temperature, Figure 4 gives for comparison results of a model published by Chambe (1978). The wavelengths observed with various two-dimensional instruments are indicated at the bottom of the figure.

Chambe's model provides radio brightness temperature values deduced directly from EUV line measurements on board the OSO VI satellite, with a minimum of hypothesis. A plane-parallel model of the CCTR is extended at higher altitudes with hydrostatic corona. For a coronal hole, the temperature is 8 10^5 K, on the basis of the differential emission measures of the EUV lines. Note that this value is in agreement with the coronal hole electron temperature obtained from recent observations from the SOHO spectrometers (CDS and SUMER) at 1.1 $R_\odot$ (David et al. 1998). In addition, to estimate refraction effects in the CCTR, different pressures have been assumed (the parameter $P_o = N_e T_e$ in cgs units indicated for each curve).

Table 1 Brightness Temperatures Measured on Coronal Holes and the Quiet Sun

Frequency (MHz)	λ (m)	Brightness Temperature Holes unit = 10^5 K	Brightness Temperature Quiet Sun unit = 10^5 K	Reference
410	.73	1.5		Coulais, 1997
408	.74	4.8		*Avignon et al., 1975*
408	.74	4.3	5.7	*Chiuderi et al., 1977 **
408	.74	4.1	5.5	*Trottet et Lantos, 1978 **
408	.74		4-4.5	Rigaud, 1991 (QS without coronal plateau)
408	.74	2.5		Lantos et al., 1992
327	.92	2.0		Coulais, 1997
317	.92		> 4.0	Shevgaokar et al., 1988 (see note 3)
236	1.27	5.5		Coulais, 1997
169	1.78	6.3		*Avignon et al., 1975*
169	1.78	6.6	8.5	*Chiuderi et al., 1977 **
169	1.78	6.3	11	*Trottet et Lantos, 1978 **
169	1.78	6.8		Alissandrakis et al., 1985
169	1.78	4.5		Lantos et al., 1987
164	1.83	4.5	5.0	Lantos et al., 1992 (QS without coronal plateau)
164	1.83	4.7		Alissandrakis et Lantos, 1996
164	1.83	5.5		Alissandrakis et Lantos, 1996
164	1.83	6.0		Coulais, 1997
160	1.88	7.3	12	Dulk et Sheridan, 1974 *
160	1.88	5.7	7.0	Dulk et al., 1977 *
160	1.88	6.4	8.5	Sheridan et Dulk, 1979 *
160	1.88	6.0	10	Sheridan et Dulk, 1979 *
80	3.75	10	12	Dulk et Sheridan, 1974 *
80	3.75	8.2	8.2	Dulk et al., 1977
80	3.75	8.0	5.2	Sheridan et Dulk, 1979
80	3.75	5.8	5.0	Sheridan et Dulk, 1979
73.8	4.07	2.0		Kundu et al., 1987
73.8	4.07	7.0	4.6	Lantos et al., 1987 (fig. 2b et 5)
73.8	4.07		1.6	Shevgaokar et al, 1988 (fig. 3)
60	5		6.0	*Aubier et al., 1971*
50	6	1.6		Kundu et al., 1987
50	6	4.2	3.0	Lantos et al., 1987
50	6		1.2	Shevgaokar et al, 1988 (fig. 3)
36.9	8.13		5.0	*Aubier et al., 1971*
30.9	9.71	1.3		Kundu et al., 1987
30.9	9.71	3.1	1.8	Lantos et al., 1987
30.9	9.71		0.7	Shevgaokar et al, 1988 (fig. 3)
29.3	10.24		3.8	*Aubier et al., 1971*

Note 1: Asterisks indicate values recalibrated or corrected for center to limb effect (see Lantos, 1980).
Note 2: References of measurements without two-dimensional instruments are in italic. This is the same for Arecibo radiotelescope (Aubier et al., 1971), which must be considered as a small instrument at decameter wavelengths.
Note 3: Shevgaokar et al. (1988) value at 317 MHz is considered here as a lower limit because figures 2a and 2b indicate zero brightness temperatures inside the solar optical disk.

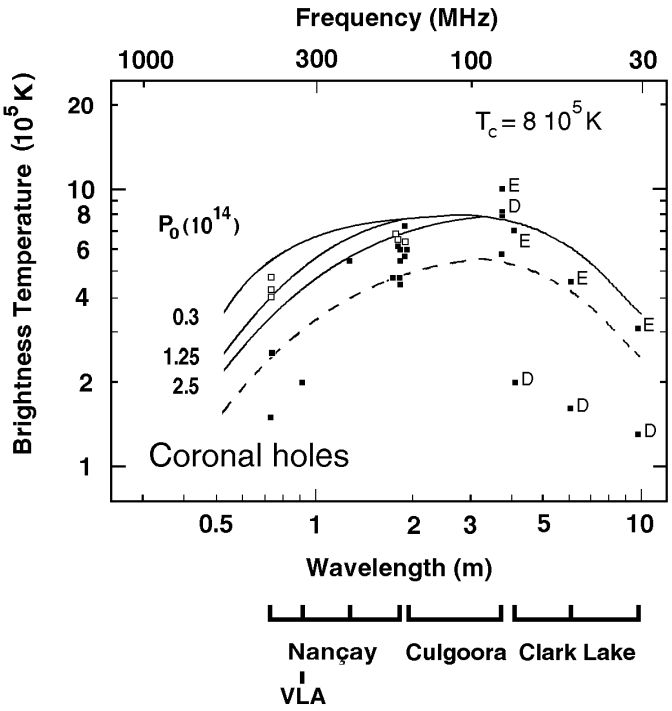

Fig. 4.. Brightness temperatures observed in coronal holes. The open squares are estimates obtained without two-dimensional observations. Decameter observations are labelled E for coronal holes seen in emission and D for coronal holes seen as brightness depressions. Chambe's model (1978) is given for comparison.

Around 160 MHz, a number of measurements is available. The mean brightness temperature of the holes is about 6 10^5 K. Three of the points obtained with the Nançay instrument are rather low (about 4.5 10^5 K) compared with the others. This is likely due to the particular characteristics of the observed holes (characteristics either intrinsic or related to their location on the disk), because the same instrument with the same calibration method gives values between 4.5 10^5 and 6.8 10^5 K. In Table 1, one notes that the first value was observed close to the solar minimum (in 1986, Lantos et al. 1992) while the second value was recorded during the solar maximum (in 1980, Alissandrakis et al. 1985). Nevertheless the number of measurements is presently not sufficient to infer some systematic variation of coronal hole brightness temperatures with the solar cycle. The brightness temperatures observed in this range are compatible with the prediction of the Chambe's model. The three points mentioned above are 30 % below the lowest model curve. This difference might be justified by uncertainties of the radio calibration (estimated from 5 % to 20 %) and by uncertainties of the model, (e.g. the EUV line intensities were not observed on the same hole as the radio data), in addition to intrinsic characteristics of the holes and their specific location on the disk.

Considering other frequencies, we see in Figure 4 that all the points are within 30 % of the model (dashed curve) except for two groups of measurements. One group, in the decimeter range, was obtained with a calibration method (Coulais 1997) which is different from that used for the other Nançay observations. Nevertheless note (Table 1) that the hole brightness temperature measured by Coulais (1997) at 164 MHz is identical to the previous measurements, and that his measurement at 236 MHz is in the same range. If the very low brightness temperatures at 410 and 327 MHz are confirmed, this would imply a strong incompatibility with a simple model of coronal hole. The second group of low brightness temperatures, compared with the model, is at decameter wavelengths. Note that they correspond to coronal holes seen as brightness depressions (Kundu et al. 1987), while the other points, obtained with the same Clark Lake instrument, are for a coronal hole in emission (Lantos et al. 1987). Thus some difference is expected between the two spectra. The low level of the brightness temperatures observed at decameter wavelengths will be discussed when quiet sun measurements will be considered (section 3.3).

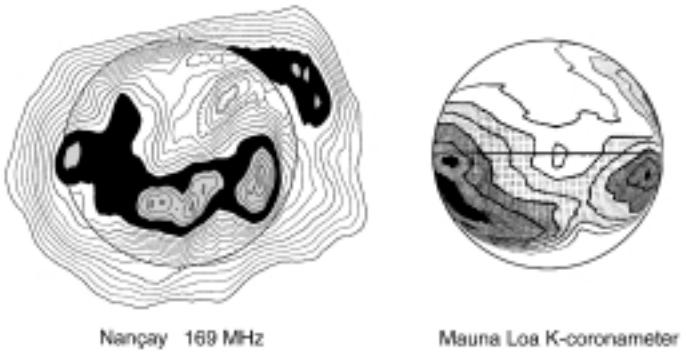

Fig. 5.. Comparison of a map at 169 MHz observed on 15 July 1984 and contours of the K-corona synoptic map projected on a sphere.

3.2. Coronal Plateau

Dulk and Sheridan (1974) found a good agreement between the shape of the corona observed beyond the limb at 160 and 80 MHz and K-corona measurements in the same range of altitudes. Synoptic maps obtained from observations beyond the limb, confirm this result at meter wavelengths (Lantos and Alissandrakis 1986) as well as at decameter wavelengths (Kundu et al. 1987, Kundu 1987). The radio contours are very close to the contours of the K-corona synoptic maps. The same result was obtained with radio synoptic maps on the disk (Lantos and Alissandrakis 1996).

Lantos et al. (1992) pointed out that the radio sources at decimeter and meter wavelengths are located, on K-corona synoptic maps, in the region of the coronal plasma sheet (also called the streamer belt). Furthermore, on the basis of daily maps, they showed that a region of enhanced brightness (which they called "coronal plateau") surrounds almost all the thermal SVC emissions. In order to get a continuous picture of this new component over the entire sun, a range of 5 10^4 K-10^5 K, below the lowest source contour has to be taken. This work was done at 164, 327 and 410 MHz, during a period covering two Carrington rotations in 1986.

The detailed shape of the coronal plateau follows the shape of the coronal plasma sheet. Nevertheless, during this period of solar cycle minimum, the coronal plasma sheet is almost equatorial and it is much better to consider a period during which the coronal plasma sheet oscillates between solar hemispheres to differentiate from an axisymmetric density model like the one proposed by Saito (1970). Figure 5 compares a daily map obtained, at 169 MHz (Lantos and Alissandrakis 1992a) with the K-corona contours of a synoptic map (Sime et al. 1985), projected on a sphere, for the same day. On the disk, the coronal plateau is shown in black, except for the SVC sources, shown in gray. The coronal plateau has a rather constant brightness temperature except close to the western limb where, in the absence of a source like the one on the east limb, a usual center to limb effect is visible. A coronal hole in the northwest quadrant is also to be noted (hatched contours on the radio map). On this specific day, the density enhancement of the coronal plasma sheet is sufficiently strong to give birth, beyond the northwest limb, to additional radio emission also indicated in black. Note that the coronal plateau is also visible, as well as its attenuation near to the limb, on the Figure 1 especially on the maps at 337 and 410 MHz. In comparison, the X-ray image shows almost same intensities in the loops of this region and in the loops covering the rest of the quiet sun. The possible origins of the radio coronal plateau will be discussed in section 4.2.

3.3. The Background Quiet Sun

We shall discuss, in this section, characteristics of the quiet sun regions outside the coronal plateau and coronal holes. Figure 6 gives the observed brightness temperatures. Open crosses are estimates obtained without two-dimensional observations. As the variations of brightness temperatures with the solar cycle are unambiguously detected around 160 MHz (Lantos et al. 1992), the values obtained by the Nançay Radioheliograph are summarised by their range rather than given as individual points. These values (as well as Rigaud's value at 408 MHz) are explicitly given without the coronal plateau contribution, which might be included in the other measurements.

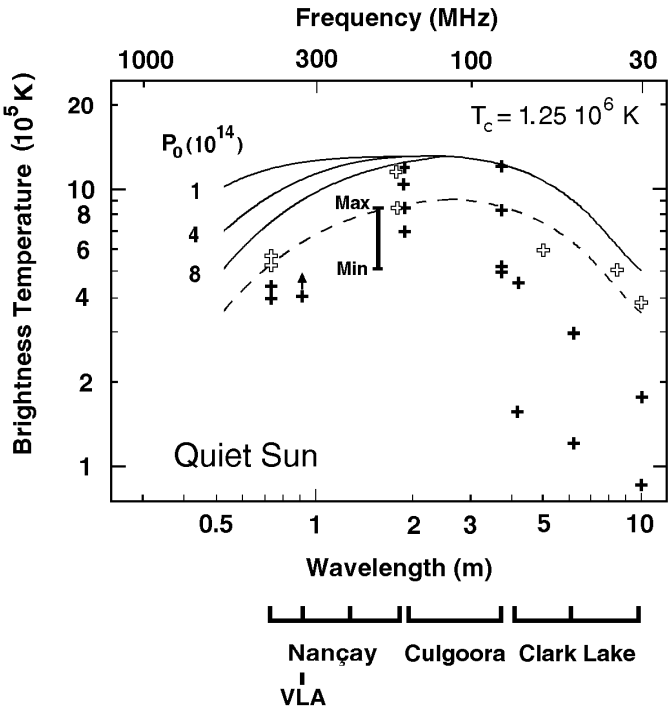

Fig. 6.. Brightness temperatures observed in the quiet sun. The open crosses are estimates obtained without two-dimensional observations. Chambe's model (1978) is given for comparison.

The predictions of the model proposed by Chambe (1978) for this component are also given on Figure 6. The coronal temperature estimated from EUV line intensities (observed with OSO VI satellite) is 1.25 10^6 K. It is in agreement with the electron temperature deduced between 1.05 and 1.10 solar radii by David et al. (1998) from SOHO observations. As in the case of a previous discussion (see section 3.1), we have plotted on the figure a dashed line which is 30 % below the lower curve of the Chambe's model. Comparison with the observed points shows that the measurements with Nançay and Clark Lake instruments, as well as Culgoora measurements, are at or below this limit. Particularly low on Figure 6 are the measurements at decameter wavelengths by Shevgaonkar et al. (1988) during the minimum of the solar cycle (February 1987). For a similar period (September 1986), Thejappa and Kundu (1992) find even much lower peak brightness temperatures of 6 10^4 K at the three Clark Lake frequencies, with a calibration precision claimed to be 20 %.

A comparison with other instruments would be extremely helpful to validate the Clark Lake results during the cycle minimum. We can only mention that during the minimum of 1976, Abranin et al. (1982) measured peak brightness temperatures of about 2 10^5 K at 25 MHz with the Kharkov instrument and that Sastry (1994) found some days with peak brightness temperatures lower than 2 10^5 K at 34.5 MHz with the Gauribidanur instrument. Note that these two instruments have an angular resolution much lower than the others. Future observations at 38 MHz with the Giant Meterwave Radio Telescope (Swarup et al.,1991) will be useful to resolve the important problem of the lowest brightness temperature of the quiet sun at decameter wavelengths. Whatever the answer, Figure 6 shows that most of the measurements of the quiet sun, from decimeter to decameter wavelengths, are not compatible with the simple plane-parallel model developed by Chambe (1978). At the same time, the observed center to limb effect on the quiet sun strongly differs from the profile predicted by plane-parallel models of the corona and of the CCTR. At meter and decimeter wavelengths the disk is rather flat and the limb brightening predicted by simple models (starting with Smerd 1950) is not observed at long decimeter wavelengths.

Scattering on small-scale inhomogeneities has been introduced in models (Scheffler 1958, Fokker 1966, Aubier et al. 1971, Riddle 1974, McMullin and Helfer 1977, Hoang and Steinberg 1977), in particular to explain low brightness

temperatures observed at decameter wavelengths. At higher frequencies it is clear since Skylab and now with Yohkoh, SOHO and TRACE, that medium-scale inhomogeneities (i.e. loops structure) must be introduced to improve the models of the background quiet sun but the task is difficult because many parameters remain unknown.

4. Medium Scale Structures

The slowly varying component at low frequencies has not a unique origin like in centimeter and short decimeter ranges where it emanates from sunspots and active regions. At longer wavelengths, there is no thermal emission in loops located above sunspots because the density of the loops is larger than the critical density of the radiation (Sheridan 1970, Axisa et al. 1971, Alissandrakis et al. 1985). This is visible on Figure 2, where dots on the 169 MHz map represent the locations of the sunspots. Specific emissions in larger loops directly above active regions seem to be limited to 410 MHz, where intense X-ray loops have thermal counterpart on radio maps (Lantos et al. 1995), as also shown on Figure 1. Nevertheless in addition to noise storm continua, a number of structures are emitting at lower frequencies, slowly varying sources which are very similar and which must be considered as full part of the SVC. Thus it would be hard today to subscribe to the statement of Sheridan and McLean (1985) who attribute radio sources uniquely to noise storm continua and write: "At metre and decametre wavelengths, especially below about 200 MHz, the slowly varying component of radiation is absent".

4.1. Coronal Streamers

The meter and decameter wavelengths are the only spectral ranges where coronal streamers are seen on the disk. This is an important advantage because this is the only method available to study precisely the relationship between streamers and underlying photospheric and chromospheric structures.

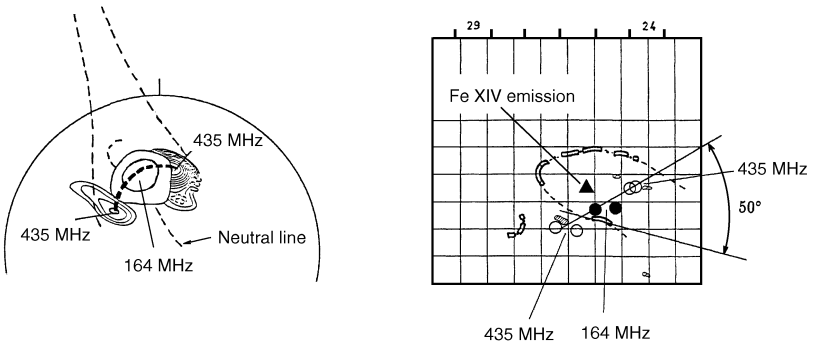

Fig. 7.. Emissions at decimeter and meter wavelengths observed on 25 October 1987 (Nançay Radioheliograph). On the left side: location on the solar disk and on the right side: comparison to the Meudon chromospheric synoptic map.

At long decimeter and meter wavelengths, coronal streamers don't give rise to sources beyond the limb as in decameter wavelengths. Streamers crossing the sky plane are seen at 169 MHz as changes in the shape of the corona. This explains the similarity of the shape of the corona at meter wavelengths and in the green coronal line (Alissandrakis et al. 1985). On the disk, very few coronal streamers have been studied in detail at long decimeter and meter wavelengths, because only a few are sufficiently isolated. Figure 7 (Lantos and Alissandrakis 1992b) shows the first example observed in 1987 with the Nançay Radioheliograph. On the left side of the figure, one source at 164 MHz and two sources at 435 MHz are shown on the solar disk. The 164 MHz source is above a photospheric neutral line while the 435 MHz sources straddles the neutral line so the most likely interpretation is in terms of a loop system emitting at decimeter wavelength in a region above the footpoints and at meter wavelength around the top of the loops. When the sources are placed (on the right of Figure 7) in the frame the corresponding Meudon synoptic map (Martres et al. 1988), they are found close to an Hα filament and close to the location of the maximum brightness of an Fe XIV emission seen, a few days before, on the eastern limb.

As mentioned above, a specific interest of observations on the disk is that the direction of the loops may be compared with the direction of the neutral line. Here an angle of 50° is found. Assuming loops with circular shape, the distance of the footpoints corresponds to an altitude of the top of the loop of about 0.25 $R_\odot$. This evaluation is compatible with the altitude of loop systems seen in streamers during eclipses (Saito and Hyder 1968). Another example has been published by Dulk and Sheridan (1974), involving this time one source at 80 MHz and two sources at 160 MHz. The double source was interpreted as split by the presence of a cavity located above the Hα filament. An alternative explanation in terms of loop system gives altitudes compatible, like for the first example, with the eclipse observation mentioned above.

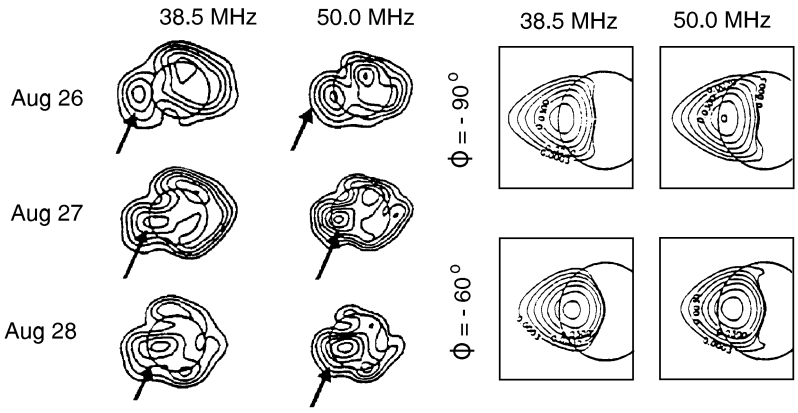

Fig. 8.. A coronal streamer observed in 1985 at 38.5 and 50 MHz with the Clark Lake Radioheliograph (left). Model of coronal streamer emission at the same frequencies (right).

Seen beyond the limb, the streamers at decameter wavelengths often appear as emission sources (Lantos et al. 1987, Kundu et al. 1987). A good example of transit of a coronal streamer from the eastern limb to the western limb has been published by Schmahl et al. (1994). A part of their observations are given on Figure 8, showing coronal streamer emissions beyond the limb as well as on the disk at 38.5 and 50 MHz. On the right side of the figure, models computed by the same authors are given for comparison. A number of other streamer models (Riddle 1970, Sheridan and McLean 1985, Thejappa and Kundu 1994, Chiuderi-Drago 1994, Alissandrakis 1994) have been computed without and with scattering effects.

4.2. Origin of the coronal plateau

The origin of the coronal plateau (section 3.2) can now be shortly discussed in the light of observations and models of coronal streamers. Chiuderi-Drago (1994) has shown that her model of streamers (which does not include a denser loop system at the base of the streamer) could explain additional brightness temperature of about 10^5 K at frequencies from 410 MHz to 164 MHz. Thus according to her the coronal plateau is due to the overdensity in the sheet of the streamers of the streamer belt. Nevertheless, (1) observation of isolated streamers (Lantos and Alissandrakis 1992b) shows that the emission geometry most likely corresponds to the loop system of the streamer rather than to the overdense part at higher altitudes, (2) the presence of center to limb effect on the coronal plateau implies a relatively low altitude of the emission, if it is due to refraction of the rays far from the disk center and, (3) there is a better agreement between radio synoptic maps on the disk and K-corona synoptic maps at 1.3 $R_\odot$ than with K-corona synoptic maps at 1.7 $R_\odot$ (Lantos and Alissandrakis 1996). This is a relevant point because, according to K-corona observer experience (e.g. Sime and McCabe 1990), proper identification of streamers needs high altitude (i.e. Sun distance of 1.7 $R_\odot$) observations. The K-corona features called "bright points" by Sime and McCabe, as well as the Fe XIV green corona structures below 1.3 $R_\odot$, are rather due to emission of denser loop systems. For these reasons, we prefer, at least provisionally, to attribute the plateau enhanced emission (streamer being present or not) to loops straddling the large-scale neutral line. Hakamada (1987) has illustrated (Figure 9) this loop system by computing potential extrapolation of the photospheric magnetic field.

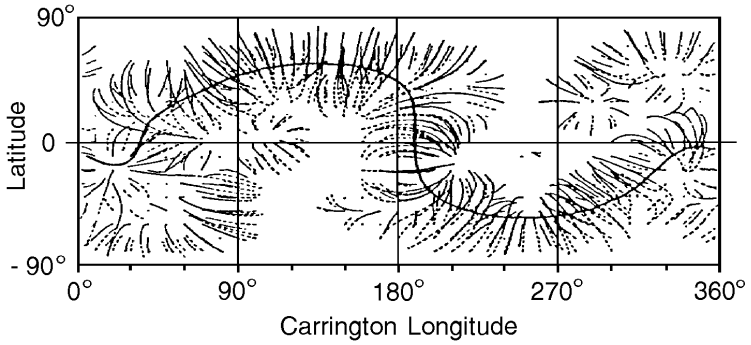

Fig. 9.. Large scale coronal loops straddling the main neutral line (current free extrapolation of photospheric magnetic field.)

4.3. Faint Noise Storms

Sheridan (1970) has published a first example of an emission source at 80 MHz identified as a faint noise storm continuum. This work was extended to 169 MHz (Alissandrakis et al. 1985) thanks to observations of Type I bursts with the high time resolution mode of the Nançay Radioheliograph. During the maximum of the solar cycle, this non-thermal component is an important part of the SVC at meter wavelengths. In the long decimeter range, faint noise storms could also be identified. Faint noise storms cannot be detected with radiospectrographs that do not have enough sensitivity. Except for their intensity and the very small number of Type I bursts, they have the characteristics of stronger noise storms well described in the scientific literature (Lesqueren 1963, Clavelier 1967, Elgarøy 1977, Kai et al. 1985). They are similarly located, not directly above the sunspot groups, but in their surroundings in loops anchored in active regions (Lesqueren 1963, Lantos-Jarry 1970).

Faint noise storms at meter wavelengths are the only source of SVC seen well beyond the limb (like for example at 1.6 $R_\odot$, according to Lantos and Alissandrakis 1998). Also characteristic is their variability in intensity and location. The brightness temperature of the faint noise storm continua at meter wavelengths is only about one million degrees (Alissandrakis et al. 1985), compared with the others which could be as bright as 10^9 K (Kerdraon and Mercier 1983). Each day, we were only able to detect a few faint Type I bursts compared with the thousands observed in stronger noise storms (Elgarøy 1977). From a comparisons of meter and decameter maps (Lantos et al. 1987), number of CLV sources at 73.8 and 50 MHz have been suspected to be noise storm continua.

4.4. Other medium-scale structures

At decameter wavelengths, the slowly varying component seems to have three origins: streamers, coronal holes, when they are in emission, and faint noise storms. Some sources located close to the poles have been tentatively interpreted as thermal or non-thermal emissions of polar plumes (Gopalswamy et al. 1992). An alternative interpretation might be in terms of coronal hole emission. At long-decimeter wavelengths and at meter wavelengths, most of the sources observed during periods far from the cycle maximum could not be explained by noise storm continua or by loops underlying coronal streamers. In presence of a still rather limited number of data, a specific statistical method has been proposed by Alissandrakis and Lantos (1996) to identify the relationship of these sources with chromospheric and photospheric features. As already suspected in previous works done with the Nançay two-dimensional observations, one association is with the photospheric neutral lines. The new fact is that the sources are not necessary located directly above the neutral line. The same method applied to faculae (Lantos et al. 1997) confirms a previous result (Lantos and Alissandrakis 1994a), suggesting the association of the sources with facula borders, the sources being outside the chromospheric faculae. Thus the studied sources are in general located between facula borders and neutral lines. A model illustrated by Figure 10 (Lantos and Alissandrakis 1998), could thus be proposed with steady loops anchored on the one side in the facula and on the other side in a region of inverse polarity of the quiet sun. The loops located *inside* the faculae have too low altitudes (or too high densities) to emit at meter wavelengths but they could be seen at 410 MHz (Figure 1).

During the minimum of the solar cycle, in the absence of faculae, sources are still present (Lantos et al. 1992). They are located above photospheric magnetic field neutral lines and thus were attributed to denser loops straddling

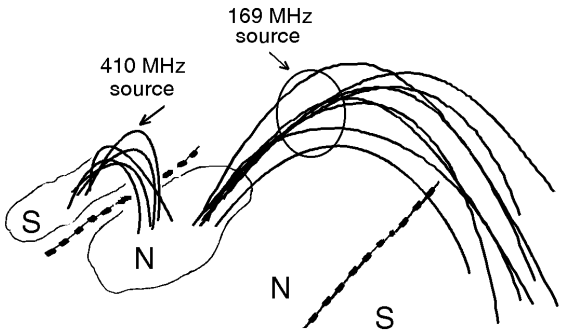

Fig. 10.. Location of emissions at different frequencies in large loops anchored into facula.

the neutral lines and possibly to streamers.

Some radio sources are located above Hα filaments (as in the case of isolated streamers), but the statistics mentioned above shows that this is not, at 169 MHz, a general rule. At 327 MHz, Lang and Willson (1989) have found emissions above two Hα filaments with the VLA. At the same frequency, Delouis (1998) has recently detected, with the Nançay Radioheliograph, a convincing example of brightness depression above an Hα filament (Figure 11), as this is the case at shorter wavelengths.

4.5. Variations with the solar cycle

As mentioned above (section 3.3), the brightness temperature of the background quiet sun (i.e. without the coronal plateau component) varies with the cycle at 160 MHz. Brightness temperatures are about 5 10^5 K during cycle minimum (Lantos et al. 1992) and 8 10^5 K during cycle maximum (after Alissandrakis et al. 1985). It is likely that the same will be found throughout the low frequency spectrum. Very low brightness temperatures are found, at decameter wavelengths, during the minimum of the solar cycle (section 3.3). The accuracy of the additional brightness temperature related to the coronal plateau (about 10^5 K) is not presently sufficient to detect expected variations with the solar cycle, but the shape of the coronal plateau at meter wavelengths is changing with the

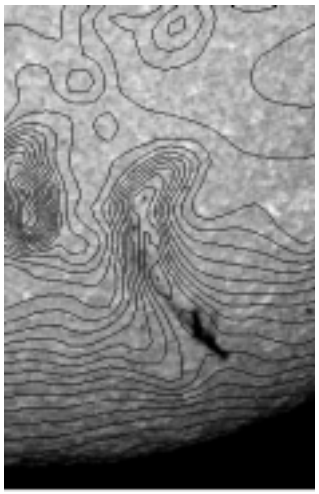

Fig. 11.. Dark Hα filament (Meudon spectroheliogram) with superposed contours at 410 MHz (Nançay Radioheliograph) showing a brightness depression.

cycle (Lantos and Alissandrakis 1994b, 1995). Equatorial during the minimum, it becomes quite complicated during cycle maximum. During intermediate phases, the coronal plateau is stable over a few Carrington rotations and oscillates from one hemisphere to the other. It follows quite precisely the evolution of the coronal plasma sheet observed with K-coronameters (Sime 1985) and of the global neutral line extrapolated from photospheric magnetic fields (Hoeksema 1984).

Finally another variation with the solar cycle to mention is the frequency of occurrence of the various components of the SVC at meter wavelengths. Faint noise storms are frequent, as expected, during solar maximum (Alissandrakis et al. 1985). During intermediate phases a number of sources is related to faculae, but noise storm continua are also present and are not easy to differentiate from the former class when the radio source is close to a sunspot group (Lantos and Alissandrakis 1998). During cycle minimum, in the absence of active regions, the SVC seems to be related to loops and streamers (Lantos et al. 1992). It is likely that at decameter wavelengths the frequency of sources related to noise storms, streamers and coronal holes is also changing with the solar cycle but no specific study has been done on this point.

5. Conclusion

When large-scale structures are considered, observations at low frequencies (from long decimeter to decameter wavelengths) are in good agreement with observations in other ranges, as well as with extrapolations of photospheric magnetic fields. Because the radio emission is more sensitive to coronal density than to temperature, the agreement is better with the K-corona rather than with coronal lines which select specific ranges of temperatures or with X-rays which correspond to loops above 2 millions degrees. When medium-scales are considered, the differences between radio and other observations are important in particular because, in the studied range, the radio observes on the disk at altitudes higher than with other techniques. The observed altitudes, as well as the possibility to trace 3-dimensional magnetic structures is of great importance in the context of the present attempts to understand better the relationship between coronal structures and solar wind regimes with applications to solar-terrestrial physics during quiescent periods. In addition to the contributions to coronal physics, this justifies efforts to continue regular observations of the quiet sun at low frequencies, in addition to observations in X-rays and EUV which are not observing the same quantities. The closure of the Clark Lake Radioheliograph in 1987, as well as the shooting of the P78-1 satellite with the Solwind coronagraph on-board, have been two ill-considered decisions with inestimable damages to solar and to solar-terrestrial physics.

References

Abranin E.P., Bazelyan L.L. and Duncan R.A., 1982, in Proceedings of STIP Symposium (M.A. Shea, D.F. Smart, D.J. McLean and G.J. Nelson eds).

Alissandrakis C.E., 1994, Adv. Space Res., 14, n° 4, 81.

Alissandrakis C.E. and Lantos P., 1996, Solar Phys., 165, 61.

Alissandrakis C.E., Lantos P., Nicolaidis E., 1985, Solar Phys., 97, 267.

Aubier M., Leblanc Y., Boischot A., 1971, Astron. Astroph., 12, 435.

Avignon Y., Lantos P., Palagi F., Patriarchi P., 1975, Solar Physics, 45, 141.

Axisa F., Avignon Y., Martres M. J. and Pick M., 1971, Solar Physics, 19, 110.

Baars J.W.M. and Hartsuijker A.P., 1972, Astron. Astrophys., 17, 172.

Bird M.K. and Edenhofer P., 1990, in Physics of the Inner Heliosphere I, (R. Schwenn and E. Marsch eds.) Springer Verlag, Berlin.

Chambe G., 1978, Astron. Astrophys., 70, 255.

Chiuderi-Drago F., 1994, in Mass Supply and Flows in the Solar Corona, (B. Fleck, G. Noci and G. Poletto eds), Kluwer Academic Publishers.

Chiuderi-Drago F., Avignon Y., Thomas R.J., 1977, Solar Physics, 51, 143.

Clavelier B., 1967, Ann. d' Astrophys., 30, 895.

Coulais A., 1997, Thèse Université Paris VII, Cartographie de la couronne solaire en ondes radioélectriques.

David C., Gabriel A.H., Bely-Dubau F., Fludra A., Lemaire Ph., and Wilhelm K., Astron. Astrophys., 336, L90.

Delouis J.M., 1999, Thèse Université Paris VII, Interfrométrie radio appliquée à la mesure des structures transitoires de la couronne solaire.

Dulk G.A. and Sheridan K.V., 1974, Solar Physics, 36, 191.

Dulk G.A., Sheridan K.V., Smerd S.F., Withbroe G.L., 1977, Solar Physics, 52, 349.

Elgarøy E.O., 1977, Solar Noise Storms, Pergamon Press, London.

Fokker A.D., 1966, B.A.N., 18, 359.

Gopalswamy N., Schmahl E.J. and Kundu M.R., 1992, in Proceedings First SOHO Workshop, ESA SP 348
Hakamada K., 1987, J. Geophys. Res., 92, A5, 4339.
Hoang S. and Steinberg J.L., 1977, Astron. Astrophys., 58, 287.
Hoeksema J. T., 1984, Thesis, Stanford University.
Kai K., Melrose D.B. and Suzuki S., 1985, in Solar Radiophysics (D.J.McLean and N.R. Labrum,eds.), Cambridge University Press, Cambridge.
Kerdraon A. and Delouis J.M., 1997, in Coronal Physics from Radio and Space Observations (G. Trottet ed.).
Kerdraon A. and Mercier C., 1983, Astron. Astrophys., 127, 132.
Kundu M.R., 1965, Solar Radio Astronomy, Interscience Publishers, New York.
Kundu M.R., 1987, in Solar and Stellar Coronal Structure and Dynamics (R.C. Altrock ed.), Sacramento Peak Obs.
Kundu M.R., Gergely T.E., Schmahl E.J., Szabo A., Loiacono R., Wang Z., Howard R.A., 1987, Solar Physics, 108, 113.
Lang K.R. and Willson R.F., 1989, Astroph. J., 344, L73.
Lang K.R. and Willson R.F., Trottet G., 1988, Astron. Astroph., 199, 325.
Lantos P., 1980, in Radiophysics of the Sun (M.R. Kundu and T. Gergely eds.), Proceedings of UAI Symposium n° 86.
Lantos P., Alissandrakis C.E., 1986, in Coronal and Prominence Plasmas (A.I. Poland ed.), NASA Conf. Publication 2442.
Lantos P. and Alissandrakis C.E., 1992a, in Solar Wind Seven (E. Marsch and R. Schwenn eds.), Pergamon Press, Oxford
Lantos P. and Alissandrakis C.E., 1992b, Proceedings First SOHO Workshop, ESA SP 348.
Lantos P. and Alissandrakis C.E., 1994a, Adv. Space Res., 14, (4) 97.
Lantos P. and Alissandrakis C.E., 1994b, in The High Latitude Heliosphere (R.G. Marsden ed.), Kluwer Academic Publishers, Dordrecht.
Lantos P. and Alissandrakis C.E., 1995, Adv. Space Res., 16, (9) 185.
Lantos P. and Alissandrakis C.E., 1996, Solar Physics, 165, 83.
Lantos P. and Alissandrakis C.E., 1998, in preparation
Lantos P. and Avignon Y., 1975, Astron. Astrophys., 41, 137.
Lantos P., Alissandrakis C.E. and Coulais A., 1997, in Solar Terrestrial Prediction Workshop Proceedings (G. Heckman, K.Marubashi, M.A. Shea, D.F. Smart, R. Thompson eds)
Lantos P., Alissandrakis C.E. and Rigaud D., 1992, Solar Phys., 137, 225.
Lantos P., Alissandrakis C.E. and the Yohkoh Team, 1995, Adv. Space Res., 17, (4/5) 261.
Lantos P., Alissandrakis C.E., Gergely T., Kundu M. , 1987 , Solar Phys., 112, 325.
Lantos-Jarry M.F., 1970, Solar Phys., 15, 40.
Lesqueren A. M., 1963, Ann. d' Astrophys., 26, 97.
Martres M.J., Simon G. and Zlicaric G., 1988, Cartes synoptiques de la chromosphère solaire, VII, fasc. 1, Observatoire de Paris.
McMullin J.N. and Helfer H.L., 1977, Solar Physics, 53, 471.
Mercier C., 1996, Ann. Geophysicae, 14, 42.
Palagi F. and Patriarchi P., 1980, Astron. Astrophys. Suppl. Ser., 41, 129
Riddle A.C., 1970, Proc. ASA, 1, 375.
Riddle A.C., 1974, Solar Physics, 36, 375.
Rigaud D., 1991, Thèse Université Paris XI, Etude de la couronne solaire aux longueurs d'onde métriques.
Saito K., 1970 , Ann. Tokyo Astron. Obs., XII, 2.
Saito K., 1972 , Ann. Tokyo Astron. Obs., XIV, 93.
Saito K. and Hyder C.L., 1968, Solar Physics, 5, 61.
Sastry Ch. V., 1994, Solar Physics, 150, 285.
Scheffler H., 1958, Z. Astrophys. 45, 113
Schmahl E.J., Gopalswamy N., Kundu M.R., 1994, Solar Physics, 150, 325.
Sheridan K.V., 1970, Proc. ASA, 1, 304.
Sheridan K.V. and Dulk G.A., 1979, IAU Symposium n° 91 (Cambridge, USA)
Sheridan K.V. and McLean D.J., 1985, in Solar Radiophysics (D.J.McLean and N.R. Labrum,eds), Cambridge University Press, Cambridge.
Shevgaonkar R.K., Kundu M.R., Jackson P.D., 1988, Astroph. J., 329, 982.
Sime D.G., 1985, in Proceedings of ESA Workshop on Future Missions in Solar, Heliospheric & Space Plasma Physics, ESA-SP 235.
Sime D.G., Fisher R.R. and Altrock R.C., 1985, NCAR Technical Note 251.
Simon P. and Legrand J.P., 1993, in Solar Terrestrial Prediction Workshop-IV (J. Hruska, M.A. Shea, D.F. Smart & G. Heckman eds.), NOAA and AFGL, USA.
Smerd S.F., 1950, Australian J. Sci. Res., A3, 34.
Thejappa G. and Kundu M. R., 1992, Solar Physics, 140, 19.
Thejappa G. and Kundu M. R., 1994, Solar Physics, 149, 31.
Trottet G. and Lantos P., 1978, Astron. Astrophys.,70, 245.
Zirker J.B., 1977, Coronal Holes and High Speed Wind Streams, Colorado Associated University Press.